Porous zinc and cobalt 2-nitroimidazolate frameworks with six-membered ring windows and a layered cobalt 2-nitroimidazolate polymorph

Angelica Orsi,[a] David J. Price,[a] Jürgen Kahr,[a] Renjith S. Pillai,[b] Scott Sneddon,[a] Shuai Cao,[c] Virginie Benoit,[d] Magdalena M. Łozińska,[a] David B. Cordes,[a] Alexandra M. Z. Slawin,[a] Philip L. Llewellyn,[d] Ian Casely,[c] Sharon E. Ashbrook,[a] Guillaume Maurin,[b] and Paul A. Wright[a,*]

[a] EaStCHEM School of Chemistry, University of St Andrews, Purdie Building, North Haugh, St Andrews, Fife, KY16 9ST, United Kingdom.

[b] Institut Charles Gerhardt Montpellier, UMR-5253, Université de Montpellier, CNRS, ENSCM, Place E. Bataillon, 34095 Montpellier cedex 05, France.

[c] Johnson Matthey Technology Centre, Sonning Common, Reading, RG4 9NH, UK.

[d] Aix-Marseille University, CNRS, MADIREL (UMR 7246), Centre de St Jérôme, 13397 Marseille cedex 20, France.

Abstract

Polymorphs of $Zn(2\text{-nIm})_2$ (compound **1**) and $Co(2\text{-nIm})_2$ (compounds **2** and **3**) (2-nIm = 2-nitroimidazole) have been prepared by two routes: solvothermal synthesis and recrystallisation of ZIF-65(Zn/Co). Compounds **1** and **2** are isostructural, with a tetrahedrally-connected framework topology related to, but different from, that of tridymite (lonsdaleite). Single crystal X-ray diffraction analysis showed that in compound **1** (*Pccn*, Z = 8; a = 8.462(8) Å, b = 14.549(15) Å, c = 18.799(18) Å, V = 2314(4) Å^3) there is rotational disorder for two of the three crystallographically-distinct linker types, which has been investigated

computationally and by solid-state NMR spectroscopy. Detailed adsorption studies on a sample of **1** prepared by recrystallisation show 1.1 mmol g^{-1} uptake of CO_2 at 0.1 bar (25 °C) with high affinity for CO_2 over CH_4 and N_2 (adsorption enthalpies of 39.5, 26.0 and 18.5 kJ mol^{-1}, respectively). A cobalt analogue (compound **2**) with improved water stability (but lower porosity) has also been prepared. Changing the conditions of synthesis and recrystallisation gives rise to a cobalt 2-nitroimidazolate ($Co(2\text{-}nIm)_2$, compound **3**), which has a layered structure ($I4_1/amd$, a = 6.025(18) Å, c = 26.95(8) Å, V = 978.3(5) $Å^3$) containing sheets of tetrahedrally-connected Co^{2+} cations composed of four membered rings, without porosity.

1. Introduction

Zeolitic imidazolate frameworks (ZIFs) are an important sub-class of metal-organic frameworks (MOFs), possessing porosity and structural flexibility.[1-3] These have a range of potential applications, including as adsorbents for carbon capture and consequently as components in mixed matrix membranes (MMM).[4-7] In these structures, divalent cations are coordinated tetrahedrally with N atoms of imidazolate linkers, and the geometry of the metal-imidazole-metal linkages is similar in angle to that observed for the Si-O-Si unit in the tetrahedrally-coordinated frameworks of silicas and silicates, including aluminosilicate zeolites. As a consequence, diverse metal imidazolate analogues of zeolites have been prepared, including ZIFs with the ANA, SOD, MER, RHO, CHA, LTA and GME framework topologies,[8] each of which has a high pore volume with accessible cages and channels. Zinc imidazolate analogues of denser tetrahedrally-connected polymorphs of silica including quartz[9] and cristobalite[10] have also been observed experimentally, in addition to a cobalt imidazolate with a topology type similar to that of tridymite.[11] Furthermore, non-porous framework ZIF-*zni*[12], another imidazolate polymorph, is known as the densest and most

thermodynamically stable member of the ZIF family.[13] Dense ZIFs with different topologies have also been discovered by mechanochemical treatment of existing frameworks (e.g. Zn(MeIm)(*kat*) from ZIF-8(SOD)),[14] and dense amorphous-ZIFs (*a*ZIFs) have been shown to result from the application of temperature, pressure, ball milling or electrical discharge.[15,16]

While silica-based structures that have pore windows consisting of 6-membered rings (6 tetrahedral cations in the ring, 6Rs), such as sodalite (SOD),[17] cannot adsorb molecules larger than water, their ZIF analogues (e.g., ZIF-8)[18,19] can adsorb small hydrocarbons and other molecules, due to the larger size of their 6Rs and the ability of the linkers to tilt. Hence, ZIF analogues of denser silicas may possess interesting adsorption properties.

Here we describe two synthetic routes to a zinc 2-nitroimidazolate, $Zn(2\text{-nIm})_2$ (compound **1**), with a topology related to, but different from, that of tridymite. The routes we report were discovered during investigations aiming to prepare nanocrystals of ZIF-65(Zn), with the SOD topology (also named NOF-1[20]and ZIF-108[21]), for applications in mixed matrix membranes, following the methodology reported by Tu *et al*.[22] Compound **1** has been observed previously, but classed as an "unknown" without further inquiry.[22] In addition, we have investigated the crystallisation of polymorphs of $Co(2\text{-nIm})_2$. As well as ZIF-65(Co),[1] the cobalt analogue of the zinc phase mentioned above was also prepared (compound **2**), as well as a layered cobalt 2-nitroimidazolate (compound **3**). While not as widely reported as three dimensionally-connected ZIFs, layered imidazolates have received recent attention as potential precursors to ZIFs and in their own right as a component of selective membranes.[23,24] Additionally, Guo *et al*.[25] have recently reported the formation of a mixed linker (imidazole and dicarboxylate), mesoporous cobalt-based MOF/ZIF containing the 2-nitroimidazole linker and terephthalic acid.

2. Experimental

Synthesis of compound 1 by recrystallisation of nanocrystals of ZIF-65(Zn)

To produce ZIF-65(Zn), the method reported by Tu *et al.*[22] was modified. $Zn(CH_3COO)_2.2H_2O$ (0.44 g, 2 mmol) was dissolved (room temperature, 10 min) in MeOH (20 mL). 2-Nitroimidazole (2-nIm, 0.45 g, 4 mmol) was dissolved (room temperature, 10 min) in DMSO (20 mL). The Zn^{2+}/MeOH solution was rapidly added to the 2-nIm/DMSO solution giving a white precipitate immediately and further stirred (room temperature, 30 minutes). The solid was collected by centrifugation (10,000 rpm, 25 min) during which the residual solvent was decanted and fresh MeOH added (~30 mL), followed by centrifugation. The product was dried in air (room temperature, 24 h) and confirmed to be ZIF-65(Zn) by comparison of the PXRD with that of a pattern simulated from single crystal XRD data of ZIF-65 (Figure S1).[1]

To synthesize compound **1** by recrystallisation, the wet solid obtained from the centrifugation step in the production of ZIF-65 was then stirred (3 days, room temperature) in MeOH (100 mL), after which it was centrifuged (10,000 rpm, 25 min), the solvent decanted and the solid allowed to dry (room temperature, 24 h).

Synthesis of compound 1 by solvothermal means

2-Nitroimidazole (0.11 g, 1 mmol), histamine (0.07 g, 0.6 mmol) and $Zn(NO_3)_2.6H_2O$ (0.60 g, 2 mmol) were stirred (room temperature, 45 min) in MeOH (15 mL). The mixture was placed in a 40 mL Teflon liner inside a stainless steel autoclave and heated in an oven (100 °C, 3 days). The yellow solution was filtered under gravity, rinsed with MeOH (20 mL) and the resulting yellow powder was dried in air (room temperature, overnight).

EDX and CHN analyses of compound **1** are consistent with the composition $Zn(2\text{-nIm})_2$ (Found: Zn, 15.9; C, 24.8; H, 1.3; N, 28.9 (recrystallisation of ZIF-65) and Zn, 12.2 ; C, 24.5

; H, 1.4 ; N, 27.0 (direct solvothermal synthesis). Calc. for $ZnN_6O_4C_6H_4$: Zn, 22.6; C, 24.9; H, 1.4; N, 29.0%).

Synthesis of compound 2 by recrystallisation of ZIF-65(Co)

$Co(CH_3COO)_2.4H_2O$ (0.49 g, 2 mmol) was dissolved (room temperature, 30 minutes) in MeOH (20 mL). 2-Nitroimidazole (0.45 g, 4 mmol) was dissolved (room temperature, 30 minutes) in DMSO (20 mL). The Co^{2+}/MeOH solution was rapidly added to the 2-nIm/DMSO solution and further stirred (room temperature, 30 min). The dark red/brown solid was collected by centrifugation (14,000 rpm, 30 min) during which the residual solvent was decanted and fresh MeOH added (~30 mL), followed by centrifugation. The product, was dried in air (room temperature, 24 h) and observed to be ZIF-65(Co) by comparison of the PXRD with that of a pattern simulated from single crystal XRD data of ZIF-65 (Figure S2).[1]

To synthesize compound **2**, dried ZIF-65(Co) was heated in a furnace (200 °C, 6 h, 2 °C min^{-1}, N_2 gas flow) and then stirred (2 days, room temperature) in MeOH (50 mL), after which it was centrifuged (11,000 rpm, 30 min), the solvent decanted and the solid allowed to dry (room temperature, 24 h).

Synthesis of compound 2 by a solvothermal route

2-Nitroimidazole (0.06 g, 0.5 mmol), histamine (0.06 g, 0.55 mmol) and $Co(NO_3)_2.6H_2O$ (0.15 g, 0.51 mmol) were stirred (room temperature, 20 min) in MeOH (15 mL). The mixture was placed in a 40 mL Teflon liner inside a stainless steel autoclave and heated in an oven (110 °C, 3 days). The dark red/brown solution was filtered under gravity, rinsed with MeOH (20 mL) and the resulting dark red powder was dried in air (room temperature, overnight).

EDX and CHN analyses of powders of compound **2** (Found: Co, 24.1; C, 24.5; H, 1.3; N, 27.2 (recrystallisation of ZIF-65) and Co, 24.3 ; C, 28.7 ; H, 2.9 ; N, 26.1 (direct solvothermal synthesis). Calc. for $CoN_6O_4C_6H_4$: Co, 20.8; C, 25.5; H, 1.4; N, 29.7%).

Synthesis of compound 3 by recrystallisation of ZIF-65(Co)

To synthesize compound **3**, the wet solid obtained from the centrifugation step in the production of ZIF-65(Co) was then stirred (3 days, room temperature) in MeOH (100 mL), after which it was centrifuged (13,000 rpm, 15 min), the solvent decanted and the solid allowed to dry (room temperature, 24 h).

Synthesis of compound 3 by a solvothermal route

2-nitroimidazole (0.06g, 0.5 mmol), 2,6-diaminopurine (0.07 g, 0.5 mmol) and $Co(NO_3)_2.6H_2O$ (0.15 g, 0.5 mmol) were stirred (room temperature, 20 min) in DMF (7.5 mL). The dark red mixture was placed in a 40 mL Teflon liner inside a stainless steel autoclave and heated in an oven (110 °C, 3 days). The dark red/black solution was filtered under gravity, rinsed with DMF (20 mL) and the resulting dark red powder was dried in air (room temperature, overnight).

EDX and CHN analyses of powders of compound **3** (Found: Co, 13.6; C, 25.3; H, 1.3; N, 29.4 (recrystallisation of ZIF-65) and Co, 19.8 ; C, 25.7 ; H, 2.3 ; N, 26.8 (direct solvothermal synthesis). Calc. for $CoN_6O_4C_6H_4$: Co, 20.8; C, 25.5; H, 1.4; N, 29.7%).

Characterisation

Powder X-ray diffraction (PXRD) data of zinc-containing samples were collected in Debye-Scherrer (capillary) geometry from STOE STAD i/p diffractometers with primary monochromation (Cu $K_{\alpha 1}$, λ = 1.54056 Å). Prior to analysis, samples were ground to a fine powder and introduced to a 0.7 mm glass capillary. A Cobra Plus non-liquid-nitrogen

cryostream (Oxford Cryosystems) attachment was employed for variable temperature PXRD (Atmosphere: air, ramp rate 5 °C min^{-1}, 10 minutes temperature hold before each measurement, temperature range of 25-150 °C and cooling at 50 and 25 °C), and the sample was contained in a 0.7 mm quartz capillary. Additional variable temperature PXRD data were recorded on a Bruker AXS D8 Advance (parallel beam mode, reflection) with Anton Parr XRK 1000 sample chamber (Cu Kα, λ = 1.54187 Å). The sample was prepared as a pressed pellet (Atmosphere: air, ramp rate 12 °C min^{-1}, temperature range of -30 to 300 °C (no cooling data)). For cobalt-containing samples, PXRD were recorded on a PANalytical Empyrean diffractometer (reflection) with primary monochromation (Cu $K_{\alpha 1}$, λ = 1.54056 Å).

Single-crystal X-ray diffraction data for compounds **1** and **3** were collected at 173 K by using a Rigaku MM-007HF High brilliance RA generator/confocal optics and Saturn 70 CCD system, with Cu Kα radiation (λ = 1.54187 Å). Intensity data were collected using ω steps accumulating area detector images spanning at least a hemisphere of reciprocal space. All data were corrected for Lorentz polarization effects. A multiscan absorption correction was applied by using CrystalClear.[26] The structures were solved by direct methods (SHELXS-97[27]) and refined by full-matrix least-squares against F^2 (SHELXL-2013[28]). Non-hydrogen atoms were refined anisotropically, and hydrogen atoms were refined using a riding model. In the structure, the crystallographically-imposed symmetry results in positional disorder in two of the three nitroimidazolates. Multiple restraints to bond distances and angles, as well as enhanced rigid-bond restraints were required to successfully model these nitroimidazolates. Calculations were performed using either the SHELXTL[27] or CrystalStructure[29] interfaces. Crystallographic data are presented in Table 1. Crystallographic data (Table 1) for the structures of compound **1** and **3** reported have been deposited in the Cambridge Crystallographic Data Centre with CCDC reference numbers 1506974 and 1506975. The data

can be obtained free of charge from The Cambridge Crystallographic Data Centre *via* http://www.ccdc.cam.ac.uk/structures.

Unit cell parameters of compound **2** were calculated using the GSAS[30,31] suite of programmes by the comparison of the calculated PXRD pattern of compound **1** to the experimental pattern of compound **2**. The original space group and atom positions were maintained. Profile parameters were refined and the Zn atom was substituted by Co in the model.

Scanning electron micrographs were obtained from a JEOL JSM-6700F FE-SEM. Samples were sputter coated three times with gold in a Quorum Q150R ES (10 mA, 30 s and 2.3 tooling factor).

Thermogravimetric analysis (TGA) data was acquired for samples (~ 3 mg) in the temperature range 25 - 800 °C at a heating rate of 5 °C min^{-1} in flowing air on a Netzsch TGA 760. Differential scanning calorimetry (DSC) data was acquired on a Netzsch DSC 204 Phoenix Instrument for the temperature range 25-200 °C (ramp rate 10 °C min^{-1}, flowing air). Differential thermal analysis (DTA) was carried out on a Netzsch STA 449C for the temperature range 37-200 °C (ramp rate 10 °C min^{-1}, flowing air).

CHN (Carbon, hydrogen, nitrogen) elemental microanalysis was carried out at the Elemental Microanalysis Department at London Metropolitan University, UK. A Carlo Erba Flash 2000 Elemental Analyser was employed, by means of a quantitative dynamic flash combustion method. A JEOL JSM-5600 SEM combined with an Oxford INCA Energy 200 EDX was employed for metal elemental analysis of samples.

Solution-state proton nuclear magnetic resonance (^{1}H NMR) spectra were acquired from a Bruker Avance 400 (400 MHz ^{1}H) and a Bruker Avance 500 (500 MHz ^{1}H) spectrometers at ambient temperature in deuterated DMSO with/without the addition of concentrated HCl (37%) to aid dissolution. Chemical shifts (δ) were recorded in parts per million (ppm) relative

to tetramethyl silane (δ 0.0). Multiplicities are designated as singlet (s), doublet (d), triplet (t), quartet (q) or multiplet (m). Coupling constants (*J*) are provided where applicable.

Seven plausible structures of compound **1**, which differ by the orientation of the 2-nitroimidazolate groups (and so the orientation of the–NO_2 functional groups) were generated by a ligand replacement strategy starting with the initial disordered structural model as solved from the refinement of the SCXRD data. The structure models, labelled as 1, 2, 3, 4, 5, 6 and 7, were further geometry optimized in P1 symmetry by density functional theory (DFT) allowing the relaxation of the atomic positions, while maintaining the unit cell parameters to those determined experimentally (a = 8.462 Å, b = 14.549 Å, c = 18.799 Å, $\alpha = \beta = \gamma = 90$ °, V=2314 $Å^3$ for (1×1×1) unit cell). These calculations were performed using the PBE[32] functional along with a combined Gaussian basis set and pseudopotential in the CP2K package.[33-36] In the cases of carbon, oxygen, nitrogen and hydrogen a triple zeta (TZVP-MOLOPT)[37] basis set was considered, while a double zeta (DZVP-MOLOPT)[37] was applied for Zn. The pseudopotentials used for all the atoms were those derived by Goedecker, Teter and Hutter.[38] The van der Waals interactions were taken into account *via* the use of semi-empirical dispersion corrections as implemented in the DFT-D3 method.[39]

Solid-state NMR experiments were performed using a Bruker Avance III spectrometer equipped with a 9.4 T widebore superconducting magnet operating at Larmor frequencies of 100.9 MHz (for ^{13}C) and 40.6 MHz (for ^{15}N). Powdered samples were packed into 4 mm ZrO_2 rotors and rotated at MAS rates of 12.5 kHz for ^{13}C and 5 kHz for ^{15}N. ^{13}C and ^{15}N spectra were recorded using cross polarisation (CP), with a contact pulse (ramped for ^1H) of 5 ms. TPPM-15[40] or SPINAL-64[41]. ^1H decoupling was employed to improve spectral resolution, with a typical radiofrequency field strength ($\gamma B_1/2\pi$) of ~100 kHz, and a recycle interval of 1 s (for ^{13}C) and 5 s (for ^{15}N) was typically used. Chemical shifts are referenced to TMS using L-alanine as a secondary reference ($\delta(CH_3)$ = 20.5 ppm) for ^{13}C, and to

nitromethane using ^{15}N-enriched glycine as a secondary reference ($\delta(NH_3) = -347.4$ ppm) for ^{15}N.[42] Variable temperature (between 0 and 140 °C) ^{13}C CP MAS NMR experiments were carried out using a 4 mm HX probe with samples were packed into 4 mm ZrO_2 rotors and fitted with ZrO_2 caps. The temperature was controlled using a Bruker BCU-II chiller and Bruker BVT/BVTB-3000 temperature controller and heater booster. The sample temperature (including frictional heating effects arising from sample spinning) was calibrated using the isotropic ^{87}Rb shift of solid RbCl.[43]

CO_2 (25 °C) and N_2 (-196 °C) adsorption isotherms (0 - 1 bar) were measured on a Micromeritics 2020 volumetric instrument. High pressure CO_2 (25 °C and N_2 (25 °C) adsorption isotherms were measured on a Hiden IGA porosimeter. Each sample was activated under vacuum prior to adsorption measurements (later specified for each sample).

Microcalorimetry experiments and cycled adsorption isotherms of compound **1** were measured on the same device (30 °C).[44] The Tian-Calvet type microcalorimeter used to measure the enthalpies consists of two thermopiles mounted in electrical opposition. Each thermopile comprises ~500 chromel-alumel thermocouples. The adsorption isotherms were obtained using a manometric approach. Each introduction of adsorbate (point-by-point) to the sample is accompanied by an exothermic thermal effect, until equilibrium is reached. The heat flow peak with time is integrated to provide an integral (or pseudodifferential) molar adsorption enthalpy for each dose. Errors in this calculation can be estimated at ± 1 kJ mol^{-1}. The calorimetric cell (including the relevant amounts of adsorbent and gas) is considered to be an open system. In this procedure, it is important to consider that the gas is introduced reversibly. Under these conditions it is possible to determine the differential enthalpy of adsorption $\Delta_{ads}h$, via the following expression:

$$\Delta_{ads}\boldsymbol{h} = \left(\frac{\boldsymbol{dQ_{rev}}}{\boldsymbol{dn^a}}\right)_{\boldsymbol{T}} + \boldsymbol{V_c}\left(\frac{\boldsymbol{dp}}{\boldsymbol{dn^a}}\right)_{\boldsymbol{T}}$$

where dQ_{rev} = heat reversibly exchanged with the surrounding environment at temperature T, as measured by the calorimeter; dn^a = amount adsorbed after introduction of the gas dose;

dp = pressure increase; V_c = dead space volume of the sample cell within the calorimeter itself (thermopile). The term $V_c dp$ is obtained from blank experiments.

Prior to each experiment, the compound **1** (0.2 g) was outgassed *ex-situ* (200 °C for 16 h under a secondary vacuum of 10^{-3} mbar). The carbon dioxide (99.998% purity), methane (99.995% purity) and nitrogen (99.9995% purity) were provided from Air Liquide (Alphagaz, France).

3. Results and Discussion

Compound 1, syntheses

A room temperature route to nanoparticles of ZIF-65(Zn) was established using a modification of a method reported by Tu *et al*.[22] A mixture of DMSO and MeOH was used as solvent, instead of DMF and MeOH. DMSO is considered a greener solvent than DMF. The ZIF-65(Zn) crystals prepared were *ca.* 500 nm in dimension (Figure 1) and their identity was confirmed by PXRD (Figure 2). Stirring as-prepared ZIF-65(Zn) in MeOH (room temperature), gave $Zn(2\text{-nIm})_2$ (compound **1**), the main subject of this paper. PXRD (Figure 2) showed it is the same phase as that previously reported, but not studied in detail.[22]

The crystals of compound **1**, prepared by this recrystallisation route, were not large enough for single crystal analysis. However, in parallel synthetic studies investigating the co-action of imidazoles other than 2-nIm in ZIF syntheses with 2-nIm, crystals of compound **1** large enough for single-crystal XRD (SCXRD) were obtained. In these reactions, the addition of histamine to solvothermal mixtures of zinc nitrate and 2-nIm in MeOH gave single crystals

up to 70 μm in size (Figure 1), with an identical PXRD pattern to that of the crystals prepared by recrystallisation of ZIF-65(Zn), indicating the materials are the same phase.

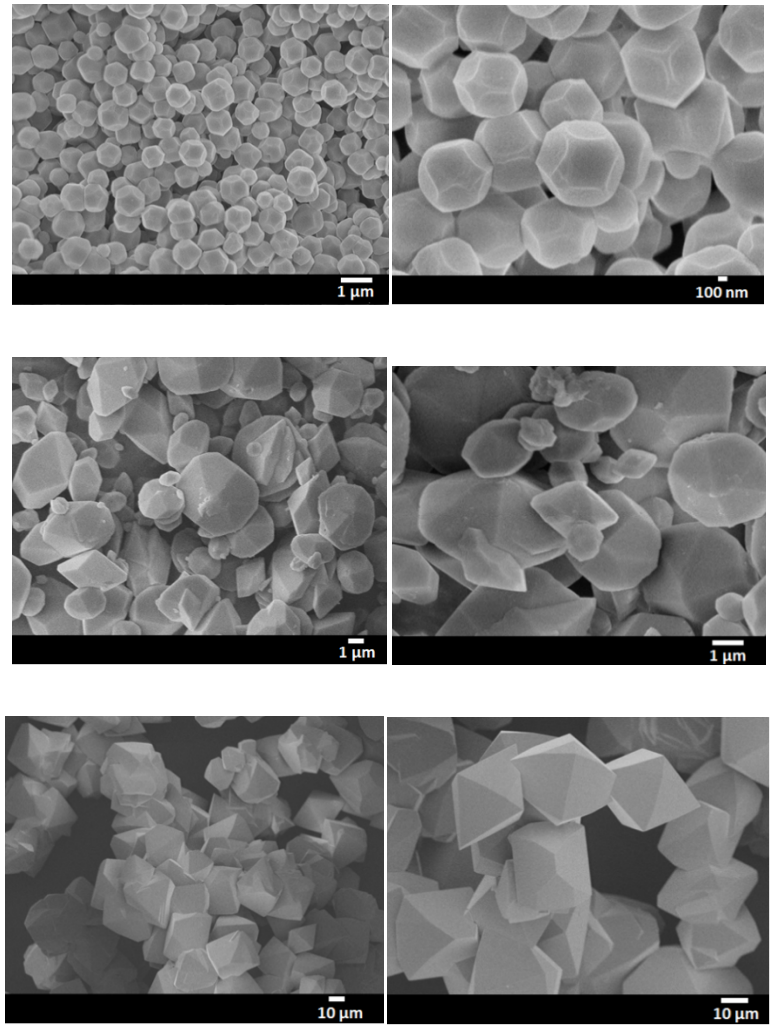

Figure 1. SEM images of ZIF-65(Zn) (top), compound **1** from the recrystallization of ZIF-65(Zn) (middle) and compound **1** from direct solvothermal synthesis (bottom).

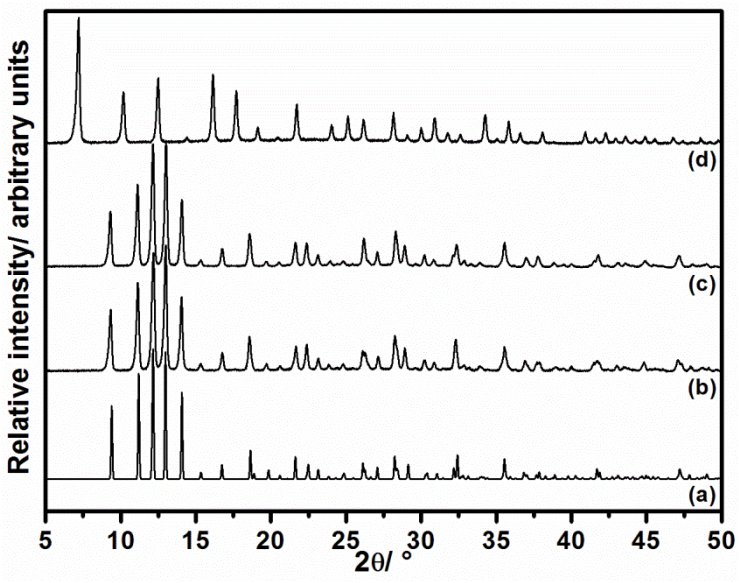

Figure 2. PXRD patterns of compound **1** from the two synthetic routes: (b) direct solvothermal synthesis and (c) recrystallization of ZIF-65(Zn), compared to (a) the simulated PXRD from single crystal XRD data of compound **1** and (d) as prepared ZIF-65(Zn).

Compound 1, characterisation

Solution-state ^{1}H NMR of digested compound **1** from the direct solvothermal route (prepared by the addition of concentrated HCl (37%) in DMSO-d_6) indicated that no histamine was present in the framework (Figures S3-S10). The role of the histamine additive in the synthesis is assumed to be a modulator – adsorbing reversibly on the surface to control growth, but not being included in the bulk structure.

The TGA traces in flowing air of compound **1** from both synthetic methods were similar, but were different from ZIF-65(Zn) (Figures S11 and S12). Compound **1** showed little weight loss (< 5%) below 80 °C, attributed to residual surface solvent, followed by a plateau to *ca.* 347 °C. Increasing the temperature above the plateau resulted in a rapid mass loss event (final mass 3-7%), hence, the expected final mass for the residue, ZnO (81.38 g mol^{-1}, final mass

28%), was less than expected. It is thought that sample may have been lost from the holder during the extremely rapid decomposition.

Gas adsorption studies for CO_2 (25 °C) and N_2 (−196 °C) of compound **1** (Figures 3 and S13) gave Type I isotherms. The CO_2 uptake on **1** prepared by recrystallisation is higher at low pressure (0.1 bar, 25 °C, conditions relevant to post-combustion flue gas) than that of ZIF-65(Zn). However, the extent of adsorption was dependent on the synthesis procedure, since the solvothermally-prepared compound **1** had significantly lower uptake, even up to 10 (N_2) and 15 (CO_2) bar pressure. The lower gas uptakes were attributed to the presence of surface impurities and associated pore-blocking, rather than differences in structure. A more detailed examination of the adsorption properties of compound **1** prepared by recrystallisation is given later, and discussed with reference to its structure.

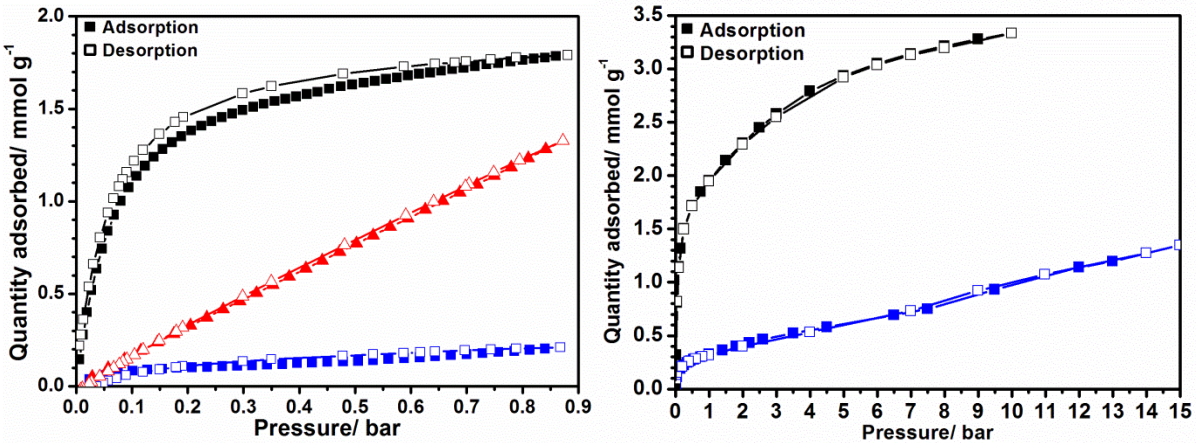

Figure 3. CO_2 adsorption isotherms (25 °C), low pressure (left) and high pressure (right), for ZIF-65(Zn) (red) and compound **1** from the recrystallisation of ZIF-65(Zn) (black) and from direct solvothermal synthesis (blue). Activation conditions: 140 °C (squares) and 200 °C (triangles) for 6 h.

To investigate the stability of compound **1** in the presence of water vapour, a sample was heated at 60 °C (18 h) in a stream of N_2 saturated with moisture at 25 °C, with no change in PXRD. Immersing samples in water (room temperature, 72 h) and refluxing in water (24 h) resulted in a different crystalline phase, which were not porous to N_2 (-196 °C) or CO_2 (25 °C). Re-immersion in MeOH (room temperature, 48 h) did not convert the structure back to compound **1**. (Figures S14-S16)

Compound 1, framework structure

The single-crystal structure of compound **1** was determined by SCXRD using crystals prepared by direct solvothermal synthesis. Details are provided in Table 1 and in the CIF. Comparison of the experimental PXRD with that simulated using the SCXRD structure shows very good agreement (Figure 2). The full framework structure is represented in Figure 4, viewed down the x-axis. The structure has one distinct Zn position and three crystallographically-unique locations for the 2-nIm linkers. The linkers in the different locations are present in the ratio 2:1:1 (ordered linker (green): disordered linker, type 1 (orange): disordered linker, type 2 (blue)). Two of these three linkers display rotational disorder, with two possible orientations for each that are related by a 180° rotation and are crystallographically equivalent. Specifically, the NO_2 groups of the ordered linkers alternate between pointing along the +y axis and then the -y axis and the NO_2 groups of the disordered linkers point randomly along +x or -x. The Zn atoms are in a tetrahedral coordination environment, the substituents being four N atoms of four independent 2-nIm linkers. Two of the coordinated linkers are of the ordered type and the other two are both the disordered linker types. Narrow channels formed by 6Rs comprised of six ZnN_4 tetrahedra and six 2-nIm linkers extend down the x-axis.

Table 1. Crystallographic data and structure refinement summary for **1** and **3**.

Compound	**1**	**3**
Empirical formula	$C_6H_4N_6O_4Zn$	$C_6H_4N_6O_4Co$
Formula weight/ g mol^{-1}	289.52	283.07
Temperature/ K	173	173
Crystal system	Orthorhombic	Tetragonal
Space group	*Pccn*	$I4_1/amd$
a/ Å	8.462(8)	6.025(18)
b/ Å	14.549(15)	6.025(18)
c/ Å	18.799(18)	26.95(8)
V/ Å^3	2314(4)	978.3(5)
Z	8	4
ρ(calcd)/ g cm^{-3}	1.662	1.922
Radiation type	Cu K_α	Cu K_α
μ/ mm^{-1}	3.141	13.988
F(000)	1152	564
R_{int}	0.0976	0.2823
GOF	1.376	1.205
Final R_1 values [$I>2\sigma(I)$][a]	0.0942	0.0977
Final wR_2 values (all data)[b]	0.2008	0.2973
CCDC number	1506974	1506975

[a] $R_1 = \sum ||F_o| - |F_c|| / \sum |F_o|$.

[b] $wR_2 = \{\sum[w(F_o^2 - F_c^2)^2] \sum (F_o^2)^2\}^{1/2}$, where $w = 1/(\sigma^2(F_o^2) + (aP)^2 + bP)$, $P = (F_o^2 + 2F_c^2)/3$.

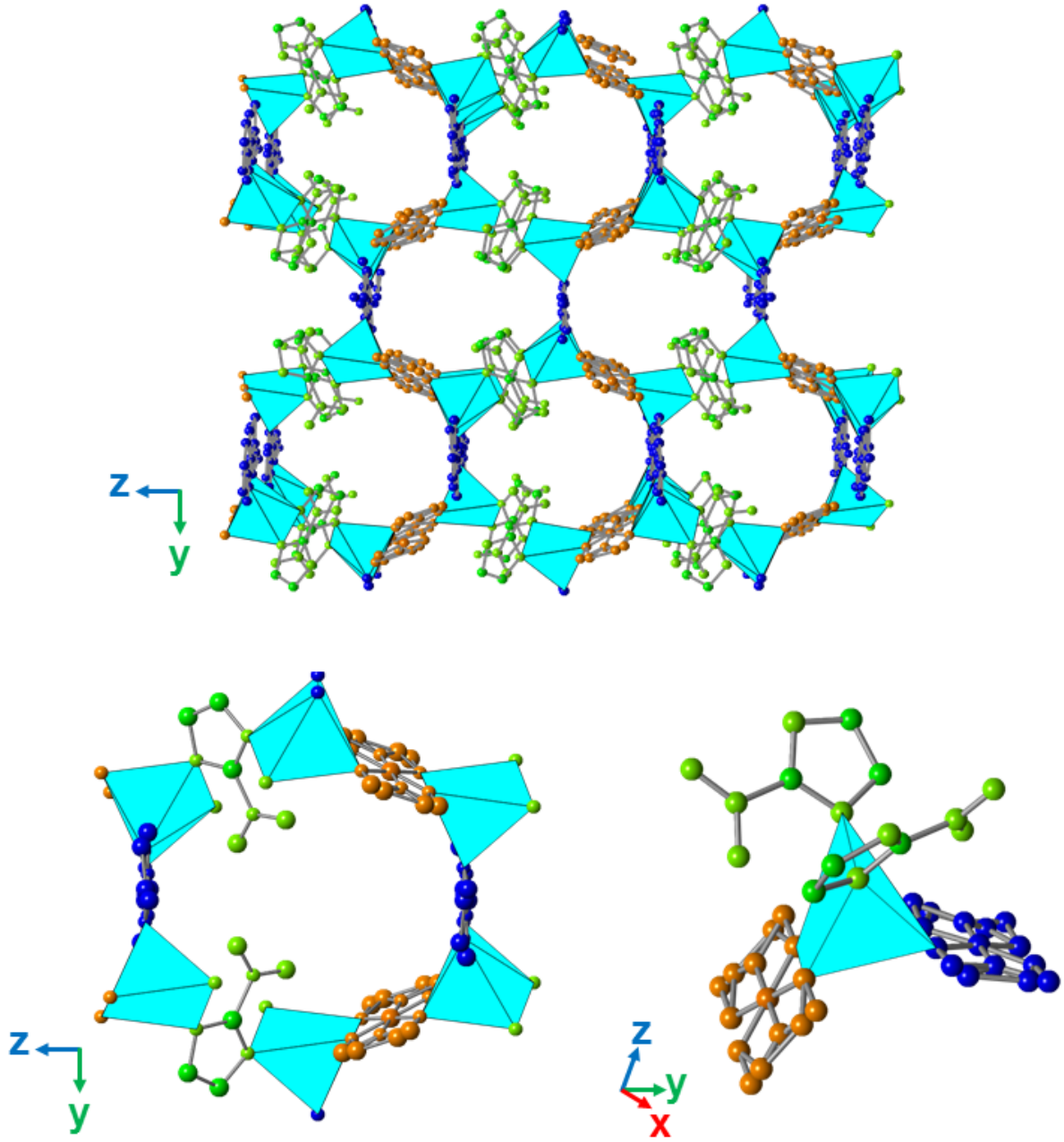

Figure 4. Polyhedral and ball-and-stick representation of the structure of compound **1**, viewed along the x-axis (top), and the constituent 6R (bottom left). The zinc(II) coordination environment in the framework of compound **1** (bottom right). Zn centres (turquoise polyhedra), ordered linkers (green), disordered linkers type 1 (orange), disordered linkers type 2 (blue). H atoms omitted for clarity.

The framework topology (Figure 5) is shown as Zn atoms that are connected by single lines representing the 2-nIm linkers. It can be considered as layers of Zn_6 rings in chair conformation, which lie parallel to the *xz* plane, themselves linked to layers above and below. The net is related to the topology types of cristobalite (diamond form of SiO_2, *dia*, 6^6 cage unit), tridymite (lonsdaleite form of SiO_2, *lon*, 6^5 cage unit) and also to that of a cobalt imidazolate $Co(Im)_2$ (6^6 cage unit) reported by Tian *et al.*[11] These nets are all built from layers of 6Rs in the chair conformation, but with different connectivity between layers. In the cristobalite and $Co(Im)_2$ topologies the orientations of the chairs in adjacent layers are similar, but the rings are distorted in $Co(Im)_2$ so that one-third of the connections between layers are to a different set of 6R nodes. By contrast, the orientations of the chairs in adjacent layers are the same for the tridymite and compound **1** structures, but whereas the links in the former structure are close to perpendicular to the layers, in compound **1** the distortion in the chairs is such that the connectivity of one-third of the linkers between layers are to different rings. The differences between the structures can be shown by comparing the cage units (Figure 5) observed in these structures (cages bounded in space by 6-membered rings which are either in chair or boat configurations). Compound **1** has a 6^6 cage, comprising four 6Rs with chair conformations (two are strongly distorted) and two 6Rs with distorted boat conformations. Metal imidazolates are already observed with the cristobalite[10] and $Co(Im)_2$[11] connectivity, with methylimidazolate and imidazolate linkers, respectively, so it is likely the sterics of groups on the imidazolate linker determines which structure is stable. Similar effects in functionalised imidazolates (2-fluoroimidazolate and 2-methylimidazolate) have been discussed previously in terms of calculated energy landscapes.[45]

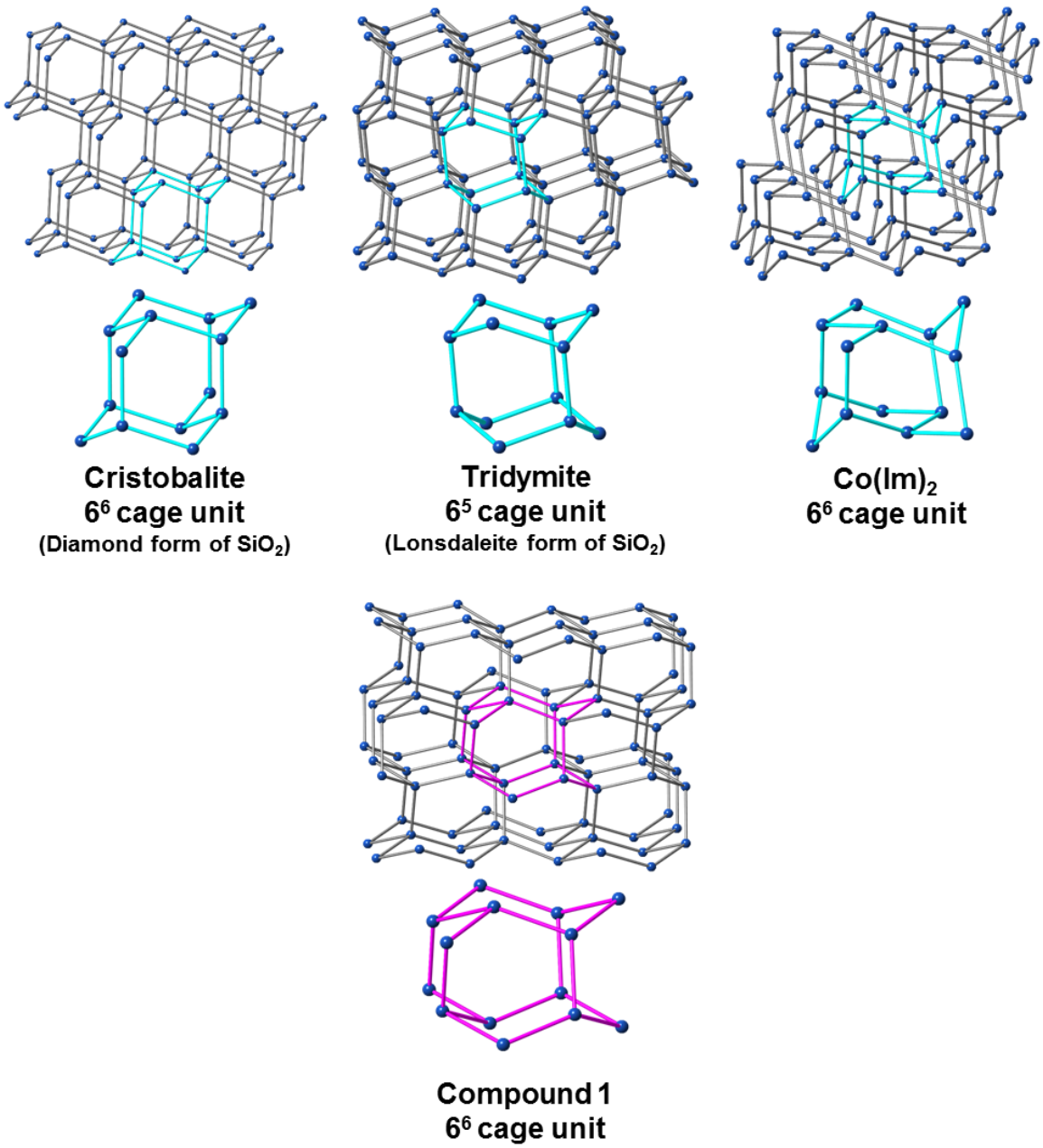

Figure 5. The networks and cage units of cristobalite (top left), tridymite (top middle), $Co(Im)_2$ (top right) compound **1** (bottom).

Compound 1, further characterisation

Seven structural models of compound **1** were generated, with various patterns of alternation of the two types of disordered linkers. The seven DFT optimized crystal structures are labelled as models 1, 2, 3, 4, 5, 6 and 7 (Figure S17) for which the total electronic energy for

each configuration was calculated (Table 2). Preliminary screening of these plausible structures of compound **1**, was performed by comparing the XRD pattern of compound **1** with those calculated for each of the seven configurations (Figure S18). Little distinction can be made between the PXRD patterns of the seven models versus the SCXRD data. The total electronic energy sequences for the models are as follows: 6<7<3<4<5<2<1. Models 1, 2, 3, 4 and 5 are the less energetically favourable structures since they correspond to the cases where neighbouring NO_2 groups of linkers are in very close proximity, leading to relatively large NO_2/NO_2 repulsion interactions, which contributes to destabilizing the structure. In contrast, the NO_2 groups in models 6 and 7 are separated by longer distances and so lead to the most energetically favourable structures - model 6 being associated with a slightly more disordered distribution of NO_2 groups. These calculations support that the most plausible configurations correspond to a disordered distribution of the NO_2 groups. The energy difference between the predicted most stable configurations, *i.e.,* model 6 and model 7 at absolute zero (4.2 kJ mol^{-1}) is only slightly higher than the thermal energy at room temperature (2.3 kJ mol^{-1}), indicating that both structures might co-exist in the synthesised sample.

Table 2. Total electronic energy for all the DFT-geometry optimized structures of the seven plausible structures and configurations of compound **1**. [a] Relative energy ranking.

Compound 1, model no.	**Energy/ kJ mol^{-1}**	**ΔE/ kJ mol^{-1} [a]**
1	-4591120.49	19.40
2	-4591133.35	6.54
3	-4591135.35	4.54
4	-4591135.20	4.69
5	-4591134.18	5.71
6	-4591139.89	0
7	-4591135.68	4.21

Solid-state NMR spectroscopic analysis of compound **1** was performed in order to investigate the short range structure. The ^{13}C CP MAS NMR spectrum of as-prepared compound **1** (Figure 6), with all resonances associated with the 2-nIm linker found between 100 and 160 ppm, confirms the aromatic nature of the linker and the presence of the diamagnetic Zn metal centre. No peaks corresponding to the synthesis solvent are found in the ^{13}C spectrum. The position of the resonances are similar to those expected for the protonated form of the isolated molecule in solution-state NMR spectra, although the exact position and number of resonances does vary, enabling a tentative partial assignment (Table 3). Peaks between 145 and 155 ppm correspond to **C**-NO_2 species, and peaks between 120 and 140 ppm correspond to **C**H species. The ^{13}C splittings arise from the presence of more than one type of 2-nIm linker in compound **1**. The two **C**-NO_2 peaks, at chemical shifts of 152.4 and 150.4 ppm, show a ratio of 1.0:2.8, consistent with a ratio of 1: (1+2), where there are crystallographically twice as many ordered linkers as each of the disordered linkers. (Ordered linker:disordered linker, type 1:disordered linker, type 2) = 2:1:1. The complex lineshape between 125 and 135 ppm can be deconvoluted using the dmfit software[46] into seven peaks (Figure S19, Table 3).

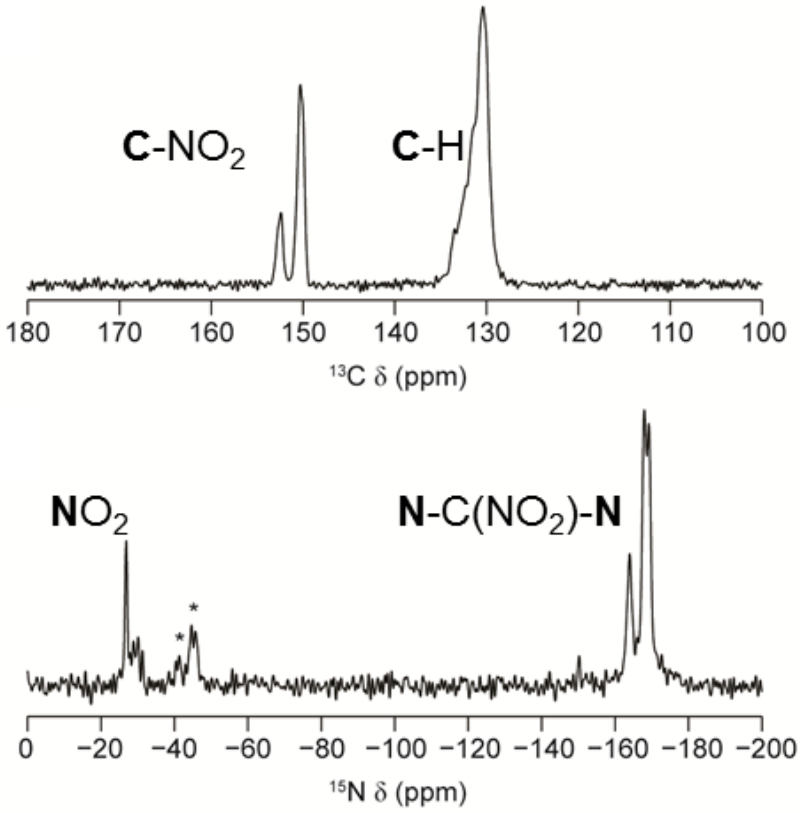

Figure 6. ^{13}C (9.4 T, 12.5 kHz MAS) (top) and ^{15}N (9.4 T, 5 kHz MAS) (bottom) CP MAS NMR spectra of compound **1**. * Spinning sidebands.

The Zn (II) metal centre in compound **1** is coordinated to four N atoms on the 2-nIm linkers. In principle, measuring ^{15}N NMR spectra should provide more information not only on the linker itself, but also the Zn coordination environment. Four main resonances are observed in the ^{15}N CP MAS NMR spectrum of compound **1** (Figure 6) and assigned to **N**O_2 species (between −25 and −30 ppm) and **N**-C(NO_2)-**N** species (between −160 and −170 ppm) (Table 3). The splitting of the ^{15}N resonances, corresponding to the **N**O_2 species, indicates that ^{15}N MAS NMR is sensitive to the crystallographic environment of the 2-nIm linkers.

Table 3. ^{13}C (9.4 T, acquired at 30 °C) and ^{15}N (9.4 T, acquired at 30 °C) NMR parameters (δ_{iso}) and assignment of the resonances of compound **1**.

	δ_{iso} (ppm)	Assignment
^{13}C		
	152.4 ± 0.1	**C**-NO_2
	150.1 ± 0.1	**C**-NO_2
	133.4 ± 0.1	**C**H
	132.7 ± 0.1	**C**H
	132.4 ± 0.1	**C**H
	131.7 ± 0.1	**C**H
	131.3 ± 0.1	**C**H
	130.7 ± 0.1	**C**H
	130.2 ± 0.1	**C**H
^{15}N		
	−26.9 ± 0.2	C-**N**O_2
	−29.7 ± 0.2	C-**N**O_2
	−163.9 ± 0.2	**N**-C(NO_2)-**N**
	−168.5 ± 0.2	**N**-C(NO_2)-**N**

Variable temperature XRD (VT-XRD) in air was performed on a sample of compound **1** prepared from the recrystallisation route (Figure 7). An initial experiment performed using a Bruker AXS D8 Advance diffractometer showed that the sample retained crystallinity during heating and all major reflections remained at similar intensities. However above 126 °C, some additional weak reflections emerged. Similar results were observed heating the sample from room temperature (25 °C) up to 150 °C in 25 °C increments and the new reflections were found to remain upon cooling. It was found that the new reflections can be indexed on the primitive orthorhombic cell (2θ 17.5° (103), 20.7° (130) and 24.3° (220)). The first of these violates the *Pccn* space group absences of the as-prepared material, indicating that a symmetry change is occurring whilst the framework structure remains intact. DSC and DTA graphs of compound **1** (Figure S20) show flat profiles for the temperature range 27-187 °C with small mass loss (1%). This suggests that the phase change observed from PXRD upon heating to 125 °C is due to dynamics of the framework.

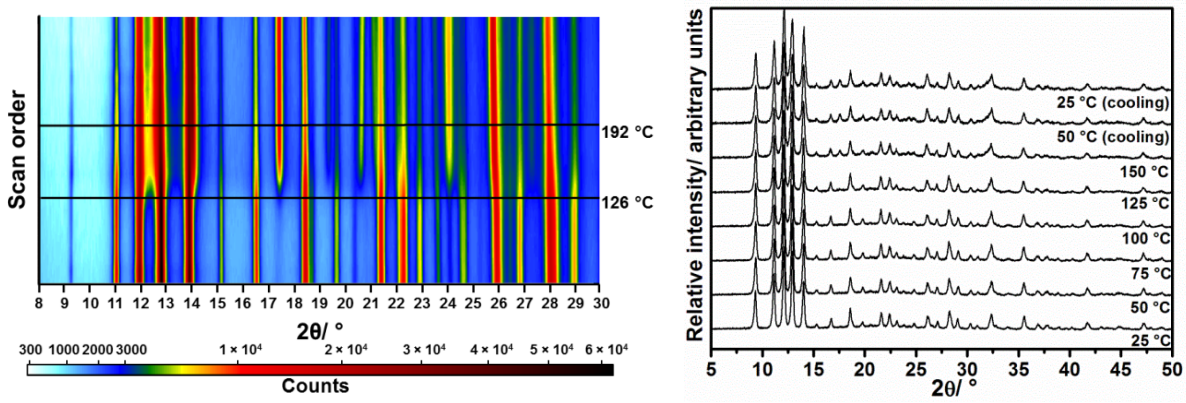

Figure 7. VT-PXRD patterns of compound **1** from Bruker diffractometer (left) and from STOE diffractometer (right).

To support the observations made by VT-XRD measurements, *i.e.*, a change in phase at higher temperatures (>126 °C), VT-NMR experiments were conducted on compound **1** with the temperature varying from 0 to 140 °C in steps of 5 °C (Figure 8). Prior to acquisition, the sample temperature was equilibrated for 300 seconds. At 0 °C, the ^{13}C spectrum of compound **1** matches closely with the ambient temperature spectrum (Figure 6), although there appears to be an additional resonance at 129.6 ppm, which decreases in intensity as the temperature of the sample increases; disappearing completely at 45 °C. In general, as the temperature of the sample increases, there are subtle changes in the position and relative intensities of the spectral resonances. This is particularly noticeable in the **C**H chemical shift region (between 120 and 140 ppm), where the peak positions of all the resonances change throughout the temperature range investigated. For the majority of the **C**H species, there appears to be a gradual decrease of the chemical shift as the temperature is increased (Figure S21). Conversely, for the **C**-NO_2 species there is a gradual increase in the chemical shift, possibly as a result of the NO_2 dynamics.

It is clear from these ^{13}C VT-NMR experiments (Figure 8) that there is no significant or sudden change in the ^{13}C spectra at higher temperature - rather a gradual and continuous change in the spectrum is observed. There are dynamic effects present in compound **1**, resulting in changes to the spectrum with temperature. Although it may be difficult to determine the exact nature and rate of the dynamic processes from these spectra, and to deconvolute the effects of dynamics from any phase transition, it does seem that a more gradual change in order/disorder is observed by NMR spectroscopy, perhaps reflecting the differences between local and long-range changes.

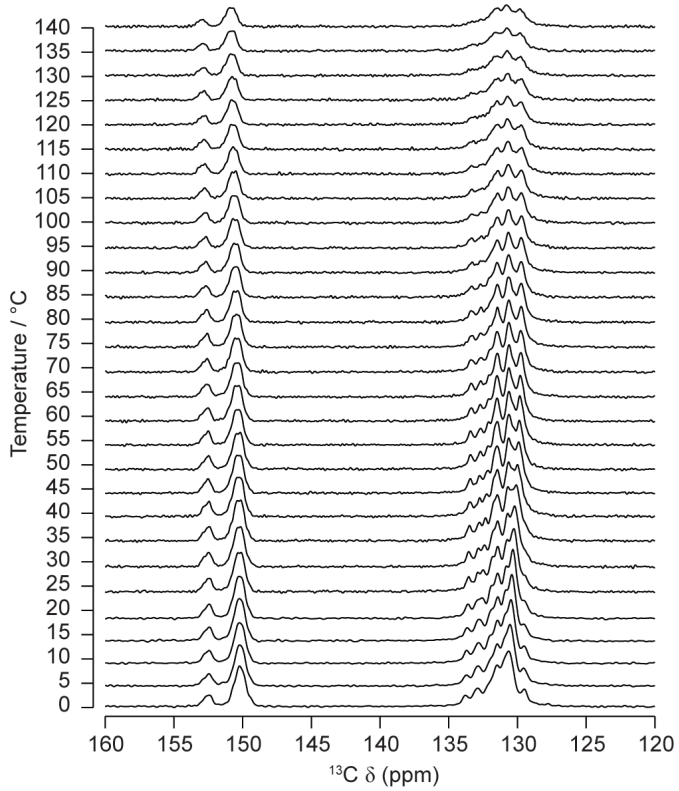

Figure 8. ^{13}C (9.4 T, 12.5 kHz MAS) VT-NMR spectra (0 – 140 °C) of compound **1**. Each spectrum is the result of averaging 1024 transients, using a recycle interval of 1 s, and ^{1}H decoupling was used during signal acquisition. Prior to acquisition, the sample temperature was equilibrated for 300 seconds.

The promising CO_2 adsorption properties of compound **1** prepared from the recrystallisation of ZIF-65(Zn) were investigated in more detail and to higher pressures. Cycling of single gas components (CO_2, CH_4 and N_2 at 30 °C, Figure 9) on compound **1** from recrystallisation of ZIF-65(Zn) with mild reactivation (30 °C, primary vacuum, 1 h) indicated that regeneration of the adsorbent was possible. At 6 bar, the uptakes are 2.9, 1.4 and 0.8 mmol g^{-1} for CO_2, CH_4 and N_2, respectively, which suggests that compound **1** has a higher affinity for CO_2 over CH_4 and N_2, consistent with the adsorption capacities at 1 bar (Table S1). In addition, at low pressures in the CO_2 adsorption isotherm there is a steep rise, which led to the determination of Henry's law constant, known as a criterion to assess the affinity. The Henry's law constant was calculated from the extrapolation of ln(n/p) versus n at low surface coverage for CO_2, CH_4 and N_2 with ratios estimated as 221 for CO_2/N_2 and 53 for CO_2/CH_4. This highlights that the framework of compound **1** has stronger interactions with CO_2 molecules compared to CH_4 and N_2.

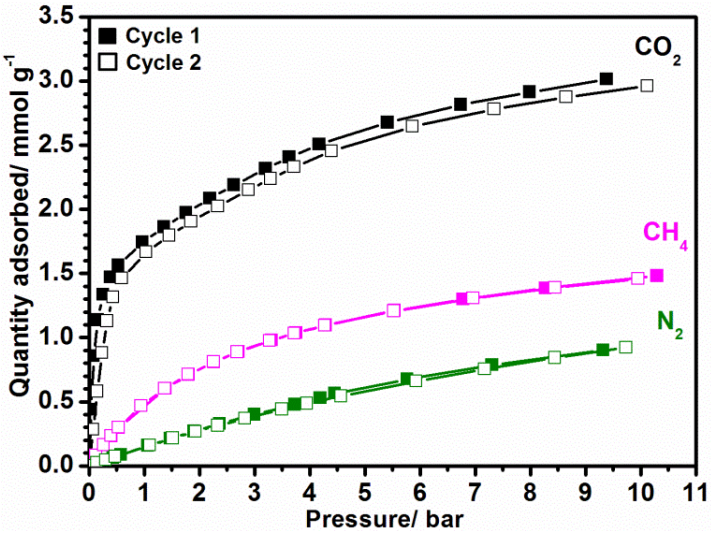

Figure 9. CO_2 (black), CH_4 (pink) and N_2 (green) single gas adsorption isotherms (30 °C, 2 cycles) for compound **1** from the recrystallisation of ZIF-65(Zn). Initial activation conditions: 200 °C, 16 h. Regeneration conditions: 30 °C, 1 h.

The prediction of selectivity (α) was estimated using IAST (Ideal Adsorbed Solution Theory)[47] calculation for post-combustion conditions (*i.e.,* 15% CO_2 and 85% N_2, 1 bar, 30 °C) and near to syngas process conditions (*i.e.*, 50% CO_2 and 50% CH_4, 5 bar, 30 °C) with resulting values of 75 and 10, respectively (Table S1). The calculated selectivity of compound **1** in post-combustion conditions exceeds those of UiO-66(Zr)-NH_2 (37), Sc_2BDC_3 (40), MIL-101(Cr) (53) and MIL-91(Al) (68), but is less than those of $Sc_2(BDC\text{-}NH_2)_3$ (120), MIL-69(Al) (120), MIL-91(Ti) (150) and MIL-53(Al)-NH_2 (877).[48]

The adsorption enthalpies obtained from microcalorimetry experiments assess the strength of interaction between the target molecules and the framework of the adsorbent. The adsorption enthalpies as a function of amount adsorbed for CO_2, CH_4 and N_2 (Figure S22), pressure range 0 to 10 bar, show relatively horizontal profiles suggesting a relatively homogeneous pore chemistry and the absence of specific features (coordinatively unsaturated sites, defects) that can be involved in the gas adsorption process. The averages of the adsorption enthalpies are 39.50 (CO_2), 26.0 (CH_4) and 18.5 (N_2) kJ mol^{-1}, in comparison to the highly selective MIL-53(Al)-NH_2, which has adsorption enthalpies of 41.5 (CO_2) 23.0 (N_2) and 12.0 (N_2) kJ mol^{-1}.[48] For compound **1**, the adsorption enthalpies confirm that the interactions of the framework are stronger for CO_2 than for CH_4 or N_2.

To identify the binding site for CO_2 molecules in the structure, the most energetically favoured system of the seven models, described and optimised in P1, was used. The interactions between CO_2 and the pore wall of compound **1** were characterized for DFT-geometry optimized model 6 (guest-loaded) considering one CO_2 molecule in a pore, where the initial location of CO_2 was arbitrarily chosen. These simulations were performed using CP2K package[33-36] at the DFT-level using the same functional and basis set as for the empty structure, where the atom positions of both compound **1** and the CO_2 molecule were fully relaxed. The resulting position of the CO_2 molecule (Figure 10) allowed the C atom (C_{CO2}) of

CO_2 to interact with the O atom (O_{NO2}) in the -NO_2 functionality of the linker, giving a characteristic $C_{CO2} - O_{NO2}$ distance of 3.32 Å. This spatial distribution leads to the O atoms of CO_2 (O_{CO2}) interacting with the H atoms (H_{linker}) of the linker with distances ranging from 2.92 to 3.21 Å.

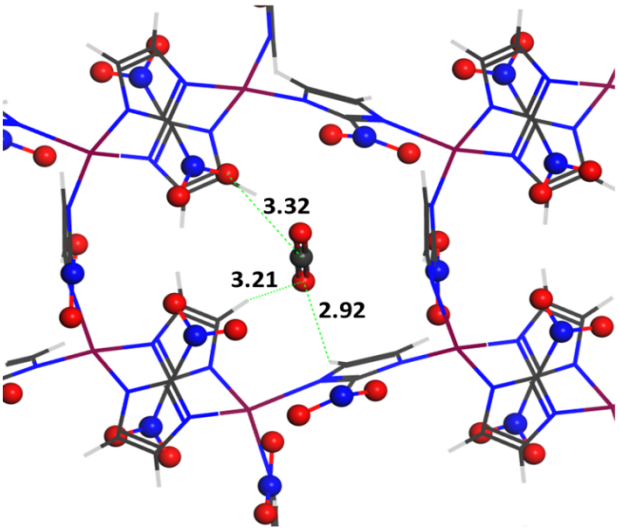

Figure 10. Local views of the DFT optimized system of CO_2 loaded compound **1** (model 6). The interacting distances are reported in Å.

Compound 2, framework structure and characterisation

Initial attempts at synthesising the cobalt analogue (compound **2**) of compound **1** included varying reaction conditions for direct solvothermal synthesis and recrystallization of ZIF-65(Co). Three polymorphs of Co(2-nIm)$_2$ were prepared during these investigations: ZIF-65(Co); the cobalt analogue of compound **1** (compound **2**); and a layered structure (compound **3**) (SEM, Figure S23; PXRD, Figure S24).

Comparison of the experimental PXRD of compound **2** with the SCXRD data of compound **1** using the GSAS suite of programs[30] allowed for a determination of the unit cell parameters of compound **2** (Figure S25). The space group (*Pccn*) and atom positions were not altered from

those of compound **1**, although Zn was replaced by Co in the model. Refinement of profile parameters, background and unit cell parameters gave *a* = 8.4897(4) Å, *b* = 14.3392(8) Å and *c* = 18.9221(12) Å (Rwp = 0.011).

TGA indicates that compound **2** has lower thermal stability than compound **1**, decomposing at 200-250 °C, but also has the rapid decomposition feature in the TGA trace (Figure S11). Compound **2** was found to retain the same structure upon refluxing in water (Figure S26). Adsorption measurements indicate that compound **2** is porous to CO_2 (Figure S27), but with lower uptake than that of the zinc analogue prepared by recrystallization of ZIF-65(Zn).

Compound 3, framework structure and characterisation

The structure of compound **3** was solved by single crystal diffraction (Table 1), and confirmed by comparison with the PXRD (Figure S28). It is composed of layers of 4Rs, in which Co(II) cations are coordinated by four N atoms from 2-nIm linkers and the orientation of the imidazolate rings alternates up and down around each 4R. (Figure 11). The CoN_4 tetrahedra are not regular, but rather distorted towards square planar. The layers have square openings with free diameters of 5.9 Å, but adjacent layers along the c axis are arranged in an eclipsed fashion, so that each layer blocks access to windows in the next. Cavities are present in the final structure, large enough to accommodate small molecules, but they are not accessible. As a consequence, compound **3** is not porous to N_2 or CO_2 (Figure S29). Nevertheless, the material extends the relatively small series of crystalline layered metal imidazolates that are known. While compound **3** prepared by recrystallisation from ZIF-65(Co) gives flat tetragonal prismatic particles a few microns across, direct synthesis give small spherical particles of similar dimensions (Figure S30). Attempts to exfoliate the plate like particles with the aim of producing porous single sheets, have so far been unsuccessful.

The thermal stability of the material from TGA (Figure S11) indicated no occluded solvent molecules were present and the decomposition of the framework at 330 °C was very rapid, similar to compounds **1** and **2**.

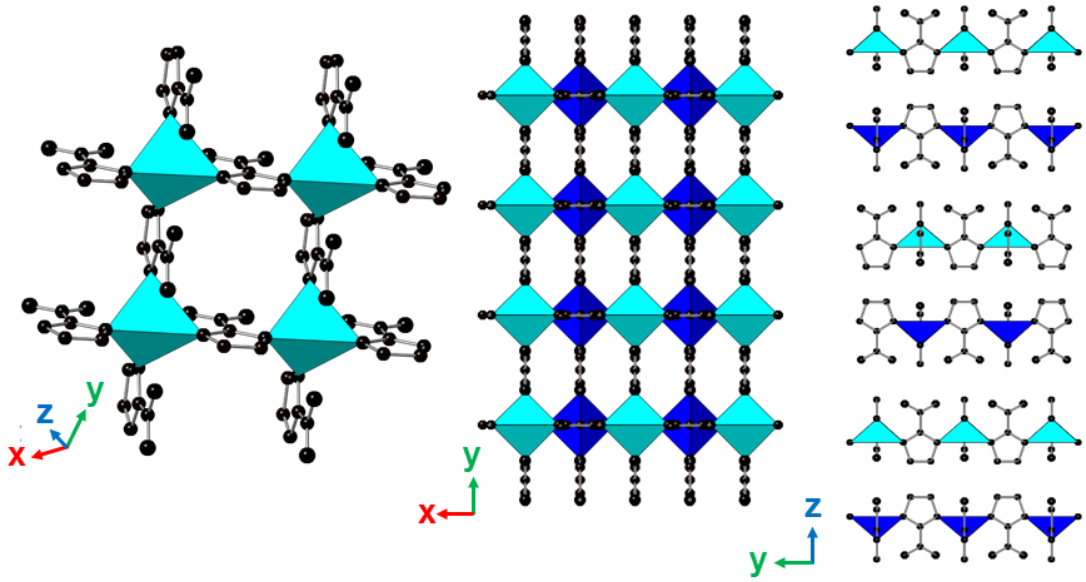

Figure 11. Polyhedral and ball-and-stick representations of the structure of compound **3**: the constituent 4R (left), eclipsing layers (middle) and individual layers along the x-axis. Zn centres (turquoise and blue polyhedral for individual layers) and linkers (black).

4. Conclusion

Direct synthesis and recrystallisation routes have been found to zinc and cobalt 2-nitroimidazolate ZIFs with a tetrahedrally-coordinated framework topology related to, but different from that of tridymite (lonsdaleite). The type of denser structure adopted by ZIFs upon recrystallisation is therefore found to be determined by the nature of the functional group on the imidazolate - other studies show highly porous Zn(methylimidazolate)$_2$ ZIFs recrystallise to the cristobalite (*dia*) topology.

Whereas silicas with 6R openings are not porous to molecules other than water, their ZIF analogues are. For example, compound **1** prepared by recrystallisation of ZIF-65(Zn) displays modest saturation uptake of CO_2 (*ca.* 3.5 mmol g^{-1}) but significantly higher CO_2 uptake at 0.1 bar and room temperature (> 1 mmol g^{-1}) than more porous ZIFs. This strong and selective CO_2 uptake is attributed, on the basis of computational simulations, to interactions between this guest with NO_2 groups on the imidazolate linkers within the narrow pores.

Currently, our attempts to prepare a cobalt analogue of the $Zn(2\text{-nIm})_2$ ZIF gives materials with lower porosity but better stability to water. Additionally, a non-porous $Co(2\text{-nIm})_2$ material has been synthesised and structurally characterised as another member of the small family of layered ZIFs, each layer of this structure comprising 4Rs including Co^{2+} with distorted tetrahedral geometry.

Acknowledgments

This work was supported by the European Community Seventh Framework Program (FP7/2007-2013) [grant agreement number 608490] (project M4CO2). A.O. would like to acknowledge the SCI for awarding a scholarship for her PhD research. G.M. thanks Institut Universitaire de France for its support. S.S. would like to thank the EPSRC for support EP/M506631/1. S.E.A would like to thank the Royal Society and Wolfson Foundation for a merit award.

Associated Content

Supporting Information is available free of charge, including PXRD patterns, NMR spectra, TGA data, adsorption isotherms and calorimetric data and SEM images. The research data

supporting this publication can be accessed at DOI: http://dx.doi.org/10.17630/773a8f44-1488-432a-985c-a2e480b529dc

References

1 R. Banerjee, A. Phan, B. Wang, C. Knobler, H. Furukawa, M. O'Keeffe and O.M. Yaghi, *Science*, 2008, **319**, 939-943.

2 B. Wang, A.P. Côté, H. Furukawa, M. O'Keeffe and O.M. Yaghi, *Nature*, 2008, **453**, 207-212.

3 D. Fairen-Jimenez, S.A. Moggach, M.T. Wharmby, P.A. Wright, S. Parsons and T. Düren, *J. Am. Chem. Soc.,* 2011, **133**, 8900-8902.

4 T. Bae, J.S. Lee, W. Qiu, W.J. Koros, C.W. Jones and S. Nair, *Angew. Chem. Int. Ed.,* 2010, **49**, 9863-9866.

5 S. Japip, Y. Xiao and T. Chung, *Ind. Eng. Chem. Res.,* 2016, **55**, 9507-9517.

6 M. J. C. Ordoñez, K. J. Balkus Jr., J. P. Ferraris and I. H. Musselman, *J. Membr. Sci.,* 2010, **361**, 28-37.

7 Q. Song, S. K. Nataraj, M. V. Roussenova, J.C. Tan, D. J. Hughes, W. Li, P. Bourgoin, M. A. Alam, A. K. Cheetham, S. A. Al-Muhtaseb and E. Sivaniah, *Energy Environ. Sci.,* 2012, **5**, 8359-8369.

8 A. P. Phan, C. J. Doonan, F. J. Uribe-Romo, C. B. Knobler, M. O'Keeffe and O. M. Yaghi, *Acc. Chem. Res.*, 2010, **43**, 58-67.

9 P. J. Beldon, L. Fábián, R. S. Stein, A. Thirumurugan, A. K. Cheetham and T. Friščić, *Angew. Chem., Int. Ed.*, 2010, **49,** 9640-9643.

10 Q. Shi, Z. Chen, A. Song, J. Li and J. Dong, *Angew. Chem. Int. Ed.*, 2011, **50**, 672-675.

11 Y. Tian, C. Cai, X. Ren, C. Duan, Y. Xy, S. Gao and X. You, *Chem. – Eur. J.*, 2003, **9**, 5673-5685.

12 R. Lehnert and F. Seel, *Z. Anorg. Allg. Chem.*, 1980, **464**, 187-194.

13 D. W. Lewis, A. R. Ruiz-Salvador, A. Gómez, L. M. Rodriguez-Albelo, F. Coudert, B. Slater, A. K. Cheetham and C. Mellot-Draznieks, *Cryst. Eng. Comm.*, 2009, **11**, 2272-2276.

14 A. Katsenis, A. Puškarić, V. Štrukil, C. Mottilo, P.A. Julien, K. Užarević, M. Pham, T. Do, S. A. J. Kimber, P. Lazić, O. Magdysyuk, R. E. Dinnebier, I. Halasz and T. Friščič, *Nat. Commun.*, 2014, **6**, Art. No. 6662.

15 T. D. Bennett, S. Cao, J. C. Tan, D. A. Keen, E. G. Bithell, P. J. Beldon, T. Friščič and A. K. Cheetham, *J. Am. Chem. Soc.*, 2011, **133**, 14546-14549.

16 T. D. Bennett and A. K. Cheetham, *Acc. Chem. Res.*, 2014, **47**, 1555-1562.

17 S. Khajavi, J.C. Jansen and F. Kapteijn, *J. Membr. Sci.*, 2009, **326**, 153-160.

18 M. T. Luebbers, T. Wu, L. Shen and R. I. Masel, *Langmuir*, 2010, **19**, 15625-15633.

19 D. Peralta, G. Chaplais, A. Simon-Masseron, K. Barthelet, C. Chizallet, A. Quoineaud and G.D. Pirngruber, *J. Am. Chem. Soc.*, 2012, **134**, 8115-8126.

20 S. Diring, D. O. Wang, C. Kim, M. Kondo, Y. Chen, S. Kitagawa, K. Kamei and S. Furukawa, *Nat. Commun.*, 2013, **4** Art. No. 2684

21 K. S. Park, PhD thesis, University of California, USA, 2007.

22 M. Tu, C. Wiktor, C. Rösler and R.A. Fischer, *Chem. Commun.*, 2014, **50**, 13258-13260.

23 Y. Peng, Y. Li, Y. Ban, H. Jin, W. Jiao, X. Liu and W. Yang, *Science*, 2014, **346**, 1356-1359.

24 R. Chen, J. Yao, Q. Gu, S. Smeets, C. Baerlocher, H. Gu, D. Zhu, W. Morris, O.M. Yaghi and H. Wang, *Chem. Commun.*, 2013, **49**, 9500-9502.

25 X. Guo, M. Wang, Y. Tang, F. Meng, G. Jiang and J. Zhu, *Cryst. Eng. Comm.*, 2016, **18**, 1768-1774.

26 *CrystalClear-SM Exper*t v2.0. Rigaku Americas, The Woodlands, Texas, USA, and Rigaku Corporation, Tokyo, Japan, 2010-2013.

27 G. M. Sheldrick, *Acta Crystallogr., Sect. A*., 2008, **64**, 112-122.

28 G. M. Sheldrick, *Acta Crystallogr., Sect. C*., 2015, **71**, 3-8.

29 *CrystalStructure* v4.2. Rigaku Americas, The Woodlands, Texas, USA, and Rigaku Corporation, Tokyo, Japan, 2013.

30 A. C. Larson and R. B. Von Dreele, General Structure Analysis System (GSAS), Los Alamos National Laboratory Report LAUR 86-748, 1994.

31 B. H. Toby, *J. Appl. Crystallogr.*, 2001, **34**, 210-213.

32 J. P. Perdew, *Phys. Rev. B*., 1986, **33**, 8822-8824.

33 J. VandeVondele, M. Krack, F. Mohamed, M. Parrinello, T. Chassaing and J. Hutter, *Comput. Phys. Commun.*, 2005, **167**, 103-128.

34 J. VandeVondele and J. Hutter, *J. Chem. Phys.*, 2003, **118**, 4365-4369.

35 G. Lippert, J. Hutter and M. Parrinello, *Theor. Chem. Acc.*, 1999, **103,** 124-140.

36 G. Lippert, J. Hutter and M. Parrinello, *Mol. Phys.*, 1997, **92**, 477-488.

37 J. VandeVondele and J. Hutter, *J. Chem. Phys.*, 2007, **127**, 114105.

38 S. Goedecker, M. Teter and J. Hutter, *Phys. Rev. B*, 1996, **54,** 1703-1710.

39 S. Grimme, J. Antony, S. Ehrlich and H. Krieg, *J. Chem. Phys.*, 2010, **132**, 154104.

40 A. E. Bennett, C. M. Rienstra, M. Auger, K. V. Lakshmi and R. G. Griffin, *J. Chem. Phys.*, 1995, **103**, 6951.

41 D. Sandström and M. H. Levitt, *J. Am. Chem. Soc.*, 1996, **118**, 6966-6974.

42 K. J. D. MacKenzie and M. E. Smith, *Multinuclear Solid-State NMR of Inorganic Materials*, Pergamon Press, Oxford, 2002.

43 J. Skibsted, H. J. Jakobsen, *J. Phys. Chem. A*, 1999, **103**, 7958-7971.

44 P. L. Llewellyn and G. Maurin, *C. R. Chim.*, 2005, **8**, 283-302.

45 I.A. Baburin and S. Leoni, *J. Mater. Chem.*, 2012, **22**, 10152-10154.

46 D. Massiot, F. Fayon, M. Capron, I. King, S. P. Le Calv, B. Alonso, J.-O. Durand, B. Bujoli, Z. Gan and G. Hoatson, *Magn. Reson. Chem.*, 2001, **40**, 70–76.

47 A. L. Myers and J. M. Prausnitz, *AIChE J.*, 1965, **11**, 121-127.

48 V. Benoit, R. S. Pillai, A. Orsi, P. Normand, H. Jobic, F. Nouar, P. Billemont, E. Bloch, S. Bourrelly, T. Devic, P. A. Wright, G. de Weireld, C. Serre, G. Maurin and P. L. Llewellyn, *J. Mater. Chem. A*, 2016, **4**, 1383-1389.